Environmental Science and Pollution Research (2019) 26:20454–20468
https://doi.org/10.1007/s11356-019-05360-2

RESEARCH ARTICLE

Magnetic nanoparticles coated with aminated polymer brush as a novel material for effective removal of Pb(II) ions from aqueous environments

Şakir Yılmaz[1] · Adem Zengin[1] · Yeliz Akbulut[1] · Tekin Şahan[1]

Received: 12 February 2019 / Accepted: 2 May 2019 / Published online: 17 May 2019

Abstract

In the present study, a poly (vinylbenzyl chloride) grafted Fe_3O_4 nanoparticle (Fe_3O_4@PVBC) was prepared by surface-initiated reversible addition fragmentation chain transfer (SI-RAFT) polymerization and subsequently coated with tris (aminoethyl) amine (TAEA). Then, Fe_3O_4@PVBC-TAEA nanoparticles were utilized as a novel adsorbent for removal of Pb(II) from aqueous media and optimal adsorption conditions were determined with response surface methodology (RSM). The used adsorbent was characterized by using X-ray photoelectron spectroscopy (XPS), transmission electron microscopy (TEM), and vibrating sample magnetometer (VSM). RSM with central composite design (CCD) was carried out to evaluate the effect of initial pH, initial Pb(II) concentration (C_0, mg/L), adsorbent dosage (mg), and contact time (min). The optimum initial pH, C_0, adsorbent dosage, and contact time were found to be 5.88, 46.51 mg/L, 17.41 mg, and 108.21 min, respectively. The maximum removal efficiency and adsorption capacity were 97.07% and 129.65 mg/g under these conditions, respectively. The kinetic data revealed that the adsorption mechanism could be best explained by the pseudo-second-order and Weber-Morris models. The isotherm studies found that both the Langmuir and Freundlich isotherm models fitted the experimental data well. The thermodynamic analysis indicated that the adsorption nature is exothermic, applicable, and spontaneous.

Keywords Adsorption · Lead · Magnetic nanoparticle · Polymer brush · Response surface methodology

Introduction

Heavy metal contamination is a significant threat worldwide for human health and the environment due to high toxicity, carcinogenicity, and non-biodegradability (Jiang et al. 2017; Rajput et al. 2016). Toxic metals such as lead (Pb), cobalt (Co), nickel (Ni), arsenic (As), and mercury (Hg) are known as the most effective sources of environmental pollution. Among these toxic metals, Pb is one of the common industrial contaminants which has harmful effects to the ecological environment. Pb pollution in aquatic media is discharged to the environment from various industrial fields including battery, mining, pigment, gasoline, paint, and metal processing. Exposure to Pb in humans can cause serious health problems such as memory problems, kidney diseases, cancer, and brain damage. The United States Environmental Protection Agency (USEPA) and the World Health Organization (WHO) have reported that the maximum concentration levels of Pb in drinking water are 0.015 and 0.01 mg/L, respectively (Afshar et al. 2016; Bagbi et al. 2017; Kumari et al. 2015; Song et al. 2018; White et al. 2009). Thus, the uptake of Pb(II) ions which are found in wastewater and drinking water has major significance because of their health and environmental risks.

Several treatment methods have been employed to uptake toxic metal ions from aqueous media, such as membrane filtration, chemical precipitation, ion exchange, reverse osmosis, and adsorption process (Ahmadi et al. 2014; Calugaru et al. 2019; Kalantari et al. 2015; Song et al. 2018; Şahan et al. 2018; Yılmaz et al. 2017). Among these technologies, the adsorption process is an effective,

Responsible editor: Tito Roberto Cadaval Jr

Electronic supplementary material The online version of this article (https://doi.org/10.1007/s11356-019-05360-2) contains supplementary material, which is available to authorized users.

✉ Tekin Şahan
tekinsahan@yyu.edu.tr

[1] Department of Chemical Engineering, Faculty of Engineering, Van Yuzuncu Yil University, 65080 Van, Turkey

Table 1 The levels and experiment ranges of the independent parameters

Independent parameters	Coded and un-coded values		
	− 1	0	+ 1
Initial pH (X_1)	2	5.5	9
Initial conc. (C_0, mg/L) (X_2)	10	55	100
Adsorbent dosage (mg/50 mL) (X_3)	5	27.5	50
Contact time (min) (X_4)	10	65	120

economical, and favorable technique due to its easy operational conditions, environmentally friendliness, and low-energy consumption (Ahmadi et al. 2014; Song et al. 2018). Furthermore, an important advantage of the adsorption procedure is that the adsorbent used to uptake heavy metal ions from the aquatic environment has high tendency and loading capacity (Kalantari et al. 2015). Various materials including bentonite, pumice, activated carbon, activated alumina, and biomaterials have been used as adsorbent in the literature for removal of Pb(II) ions from aqueous solutions (Imamoglu and Tekir 2008; Naiya et al. 2009; Naseem and Tahir 2001; Sarı and Tuzen 2009; Şahan and Öztürk 2014; Tabaraki et al. 2014). However, these materials have some disadvantage like low adsorption rate. For this reason, adsorbents which possess properties such as higher surface area, shorter equilibrium time, and smaller diffusion resistance are gaining increasing attention for uptake of heavy metal ions from aquatic media (Ahmadi et al. 2014). In recent times, magnetic nanoparticles such as magnetic magnetite (Fe_3O_4) have been considered to be an effective material for heavy metal adsorption due to the ability to quickly and easily separate them from aquatic media using a magnetic field. Thus, Fe_3O_4-based adsorbents are a wonderful way to uptake heavy metal ions from aquatic environments due to strong electrostatic attraction between Fe_3O_4 and metal ions (Kalantari et al. 2014; Kuang et al. 2013; Sadeghi et al. 2012). Moreover, magnetic nanoparticles are generally modified with self-assembled monolayer of trialkoxysilanes such as aminotri(m) ethoxy silane or mercaptotri(m) ethoxy silane for adsorption of some heavy metal ions (Banaei et al. 2015; Elkady et al. 2016; Melnyk et al. 2018). Although the preparation of the adsorbent is simple via formation of a self-assembled monolayer, the adsorbents have some limitations such as low adsorption capacity and slow adsorption kinetics. To overcome these limitations, polymer

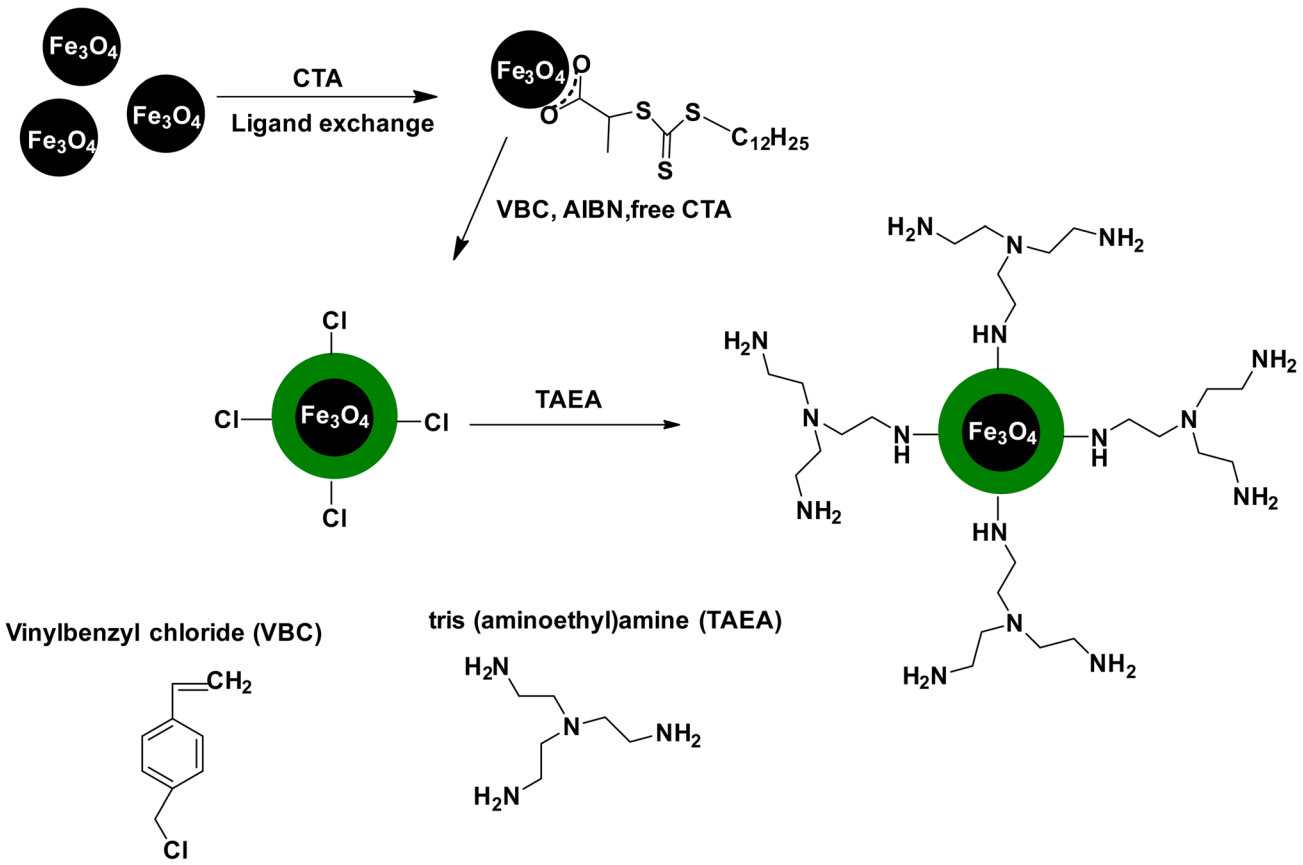

Scheme 1 Schematic presentation for the preparation of Fe_3O_4@PVBC-TAEA

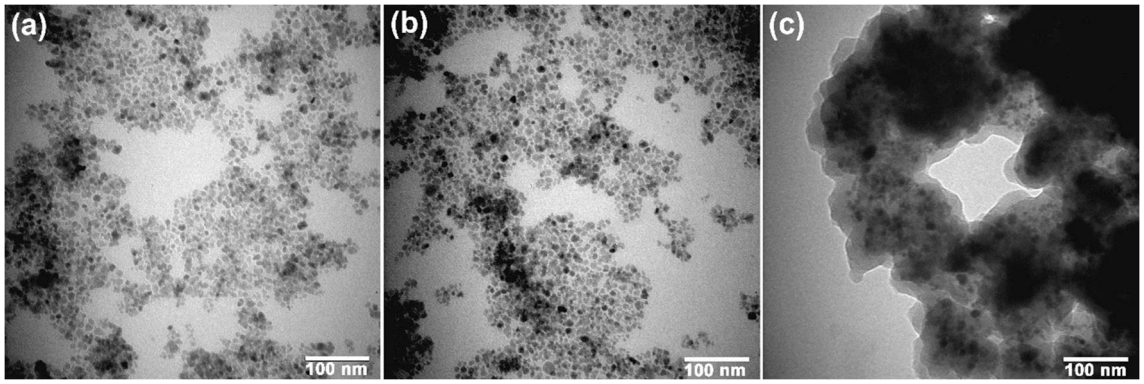

Fig. 1 TEM images of **a** bare Fe_3O_4, **b** Fe_3O_4@CTA, and **c** Fe_3O_4@PVBC-TAEA

brushes have been introduced into the adsorption technology in the last decades (Deng et al. 2012; Djouani et al. 2011; Liu et al. 2014). Generally, polymer brushes are synthesized through surface-initiated controlled/living radical polymerization techniques. Apart from the other polymerization techniques, surface-initiated reversible addition fragmentation chain transfer (SI-RAFT) polymerization is a more attractive method for the preparation of polymer brushes in terms of simplicity, mild polymerization conditions, and applicability to most monomers. Although SI-RAFT polymerization has been widely used to construct functional (bio) materials, only limited studies were performed about adsorbent preparation. Hosseinzadeh et al. (2018) synthesized poly (acrylic acid-co-acrylamide) polymer brushes on multiwalled carbon nanotubes for the adsorption of the copper(II) ions. Sánchez et al. (2018) reported that polymer-enhanced ultrafiltration membrane prepared via SI-RAFT polymerization showed high adsorption capacity and selectivity for Cr(VI). Wang et al. (2015) synthesized poly (vinyl tetrazole) resin via a combination of RAFT polymerization and click chemistry for the adsorption of Hg(II). However, as far as we know, there has been no report on the preparation of aminated PVBC-coated magnetic nanoparticles via SI-RAFT polymerization as well as its use as a sorbent for the adsorption of Pb(II).

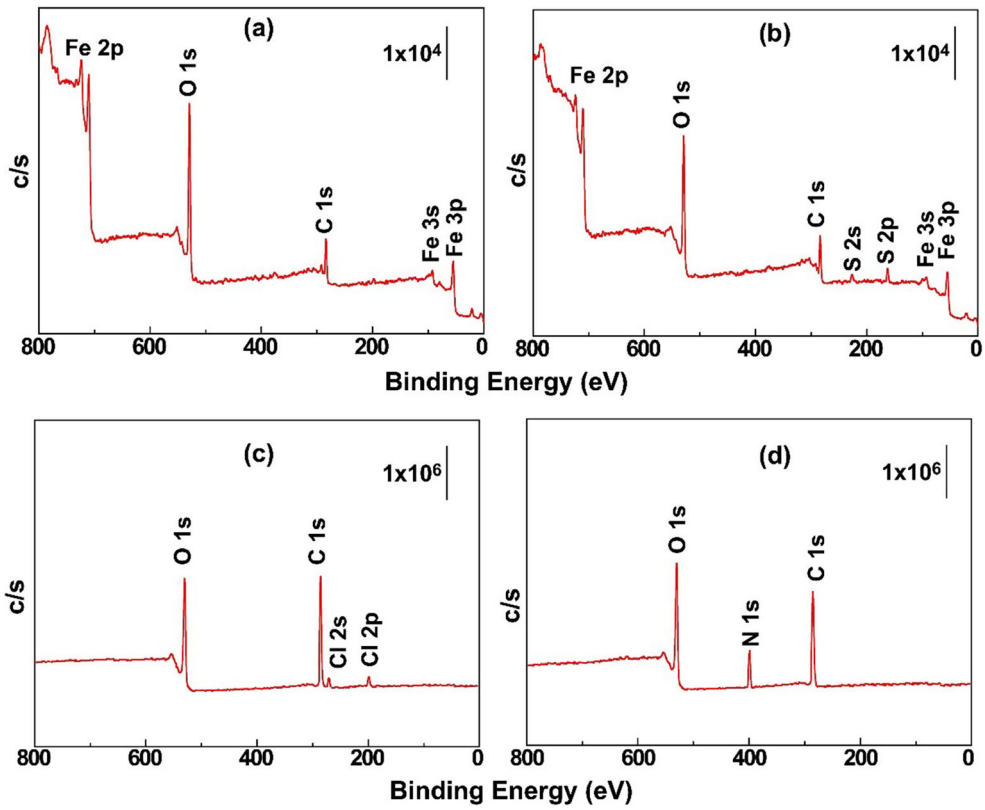

Fig. 2 XPS wide scan spectra of **a** bare Fe_3O_4, **b** Fe_3O_4@CTA, **c** Fe_3O_4@PVBC, and **d** Fe_3O_4@PVBC-TAEA

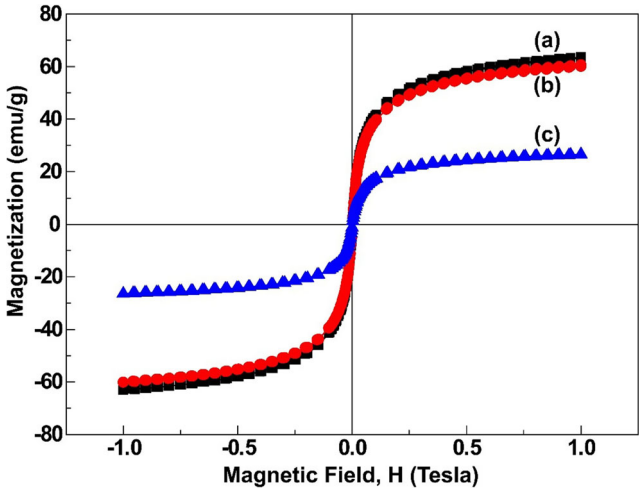

Fig. 3 VSM hysteresis loops of (**a**) bare Fe_3O_4, (**b**) Fe_3O_4@CTA, and (**c**) Fe_3O_4@PVBC-TAEA

Optimization of adsorption parameters including initial pH, initial heavy metal concentration, ambient temperature, amount of adsorbent, etc., and maximum removal of heavy metal ions by the traditional methods are impractical procedures on account of requiring numerous experiments, consuming extra materials and time. In these techniques, an independent parameter for optimization is changed, while others are fixed at a constant level. Moreover, the interactive effects among independent parameters cannot be evaluated with these methods (Antonopoulou et al. 2017; Kalantari et al. 2015; Nikraftar and Ghorbani 2016; Şahan et al. 2010). Some statistical programs used to overcome these problems have been highly significant. Response surface methodology (RSM) is a mathematical and statistical approach that is used for optimizing and designing experiments by evaluating multivariable effects of numerous independent parameters in lower numbers of tests. The main objective of the RSM application is to vary all operating parameters simultaneously and then fit the experimental data to a mathematical model (Ahmadi et al. 2014; Bezerra et al. 2008; Şahan and Öztürk 2014).

In the present research, the main objective is to investigate the influence of magnetic nanoparticles coated with aminated polymer brush (Fe_3O_4@PVBC-TAEA) as a novel adsorbent for Pb(II) ion removal from aqueous environments and to assess the optimal conditions of the most significant adsorption parameters via RSM. The adsorption performance of Pb(II) ions was examined for the most effective independent

Table 2 CCD design matrix and the corresponding responses

Run	Initial pH (X_1)	Initial Pb(II) conc. (C_0, mg/L) (X_2)	Adsorbent dosage (mg/50 mL) (X_3)	Contact time (min) (X_4)	Pb(II) adsorption (%)	The residuals (ε_n = observed − predicted)
1	2 (− 1)	10 (− 1)	5 (− 1)	10 (− 1)	25.40	5.70
2	5.5 (0)	10 (− 1)	27.5 (0)	65 (0)	81.23	6.03
3	5.5 (0)	55 (0)	5 (− 1)	65 (0)	84.32	− 2.11
4	2 (− 1)	10 (− 1)	5 (− 1)	120 (+ 1)	60.92	2.38
5	9 (+ 1)	10 (− 1)	5 (− 1)	120 (+ 1)	76.75	− 2.00
6	9 (+ 1)	10 (− 1)	5 (− 1)	10 (− 1)	50.81	− 7.67
7	2 (− 1)	55 (0)	27.5 (0)	65 (0)	84.63	− 6.51
8	5.5 (0)	55 (0)	27.5 (0)	65 (0)	94.79	2.19
9	9 (+ 1)	100 (+ 1)	50 (+ 1)	120 (+ 1)	47.12	2.87
10	2 (− 1)	100 (+ 1)	5 (− 1)	120 (+ 1)	29.01	5.12
11	9 (+ 1)	10 (− 1)	50 (+ 1)	120 (+ 1)	82.66	2.13
12	2 (− 1)	100 (+ 1)	50 (+ 1)	120 (+ 1)	17.29	4.26
13	5.5 (0)	55 (0)	27.5 (0)	65 (0)	94.73	2.25
14	9 (+ 1)	100 (+ 1)	5 (− 1)	10 (− 1)	19.71	8.59
15	5.5 (0)	55 (0)	27.5 (0)	65 (0)	94.52	2.46
16	9 (+ 1)	10 (− 1)	50 (+ 1)	10 (− 1)	65.02	3.44
17	5.5 (0)	100 (+ 1)	27.5 (0)	65 (0)	84.49	− 5.63
18	5.5 (0)	55 (0)	27.5 (0)	65 (0)	94.89	2.21
19	5.5 (0)	55 (0)	27.5 (0)	65 (0)	94.21	2.76
20	5.5 (0)	55 (0)	27.5 (0)	10 (− 1)	85.01	− 6.34
21	2 (− 1)	10 (− 1)	50 (+ 1)	10 (− 1)	55.50	− 0.95
22	9 (+ 1)	100 (+ 1)	5 (− 1)	120 (+ 1)	63.16	− 6.46
23	5.5 (0)	55 (0)	50 (+ 1)	65 (0)	93.10	− 2.51
24	2 (− 1)	100 (+ 1)	50 (+ 1)	10 (− 1)	15.30	8.56
25	5.5 (0)	55 (0)	27.5 (0)	120 (+ 1)	92.61	1.72
26	2 (− 1)	10 (− 1)	50 (+ 1)	120 (+ 1)	77.46	− 4.02
27	9 (+ 1)	100 (+ 1)	50 (+ 1)	10 (− 1)	60.67	− 6.75
28	2 (− 1)	100 (+ 1)	5 (− 1)	10 (− 1)	28.69	− 6.54
29	9 (+ 1)	55 (0)	27.5 (0)	65 (0)	92.48	2.89
30	5.5 (0)	55 (0)	27.5 (0)	65 (0)	94.86	2.48

Table 3 ANOVA results for Pb(II) adsorption

Source	Sum of squares	*df*	Mean square	*F* value	*p* value prob > *F*
Model (significant)	19,796.50	14	1414.04	13.68	< 0.0001
X_1-Initial pH	1497.52	1	1497.52	14.49	0.0017
X_2-Initial conc. (C_0)	2457.24	1	2457.24	23.78	0.0002
X_3-Adsorbent dosage (mg/50 mL)	315.36	1	315.36	3.05	0.1011
X_4-Contact time (min)	1102.46	1	1102.46	10.67	0.0052
$X_1 X_2$	123.24	1	123.24	1.19	0.2921
$X_1 X_3$	34.52	1	34.52	0.33	0.5719
$X_1 X_4$	11.72	1	11.72	0.11	0.7410
$X_2 X_3$	280.19	1	280.19	2.71	0.1204
$X_2 X_4$	296.27	1	296.27	2.87	0.1111
$X_3 X_4$	372.34	1	372.34	3.60	0.0771
X_1^2	298.65	1	298.65	2.89	0.1098
X_2^2	699.31	1	699.31	6.77	0.0201
X_3^2	289.90	1	289.90	2.80	0.1147
X_4^2	284.50	1	284.50	2.75	0.1178
$R^2 = 0.93$					

parameters including initial pH, initial Pb(II) concentration (C_0), adsorbent dosage, and contact time. Central composite design (CCD) was successfully applied to express the relationships between response (Pb(II) adsorption, %) and the adsorption parameters. This study presents a new adsorbent-adsorbate combination not previously reported in the literature. For this purpose, novel amino-functionalized polymer brush grafted magnetic nanoparticles were synthesized and characterized for the effective removal of Pb(II) from aqueous media. The great advantage of the present study is that polymer brush grafted magnetic nanoparticles showed fast adsorption kinetics, high adsorption capacity, and high recovery of Pb(II). Taking into account this information, it is believed that the constructed polymer brush containing magnetic nanoparticles will allow the development of new methods for adsorption technology.

Materials and methods

Materials

Azobis (isobutyronitrile) (AIBN, 98%, Acros Organics, USA) was recrystallized from ethanol and stored at − 20 °C. Oleic acid (OA) was also purchased from Acros Organics, USA. All other chemicals were purchased from Sigma-Aldrich (Germany) at available highest purity and used as received unless otherwise noted. The chain transfer agent (CTA), 2-[(dodecylsulfanylcarbonylthiolsulfanyl) propionic acid], was synthesized according to published procedure (Stenzel and Davis 2002).

Instruments

The morphology and diameter analysis of the magnetic samples were evaluated by transmission electron microscopy (TEM, JEOL 1400, USA). Nanoparticle dispersion of 3 μL was dropped on the carbon-coated copper grid and left to dry at room temperature. X-ray photoelectron spectroscopy (XPS) analysis was conducted with a SPECS XPS spectrometer (Germany) using Al Kα as an X-ray source. Magnetic behavior of the nanoparticles was determined by vibrating sample magnetometer (VSM) from Cryogenic Limited PPMS system (UK). The concentrations of Pb(II) were recorded with atomic absorption spectrophotometer equipment (AAS, Thermo Scientific iCE 3000 SERIES, USA).

Preparation of oleic acid capped Fe_3O_4 nanoparticles (Fe_3O_4@OA)

Fe_3O_4 nanoparticles were synthesized by co-precipitation method and modified with OA in situ as reported in an earlier study (Sun et al. 2006). Briefly, 1.17 g of $FeSO_4 \cdot 7H_2O$ and 2.05 g of $FeCl_3 \cdot 6H_2O$ were dissolved in 50 mL of double distilled deionized water. Then, 13 mL of NH_4OH (25%, *v*/*v*) was added to the solution. After stirring for 30 min at room temperature, 0.5 mL of OA was added into the solution at 70 °C and stirred for an additional 30 min. Then, 25 mL of the black suspension and 25 mL of toluene were mixed in a separating funnel. After addition of a small amount of NaCl, magnetic particles were moved to the organic phase. The Fe_3O_4@OA nanoparticles were collected by using a magnet and washed with acetonitrile (10 mL) several times, and lastly, dried under vacuum.

Synthesis of PVBC grafted Fe_3O_4 nanoparticles (Fe_3O_4@PVBC)

Fe_3O_4@OA nanoparticles of 100 mg were dispersed into 20 mL of acetonitrile with ultrasonic treatment at room temperature and 0.51 g of CTA was added into the black suspension. The mixture was stirred by a mechanical stirrer at 60 °C for 24 h under nitrogen protection. The CTA-capped Fe_3O_4 nanoparticles (Fe_3O_4@CTA) were obtained through ligand exchange reaction between OA and CTA. The Fe_3O_4@CTA nanoparticles were collected by a magnet and sequentially washed with plenty of acetonitrile (ACN), tetrahydrofuran (THF), and dichloromethane (DCM). Then, the final product was dried under vacuum and stored at + 4 °C until use.

Fe_3O_4@CTA nanoparticles of 50 mg were dispersed in 10 mL of dimethylformamide (DMF) containing 7.4 mmol VBC and 28.1 μM AIBN. The mixture was bubbled with nitrogen for 30 min in an ice-bath and then immersed into the oil bath at 60 °C for 16 h. After polymerization, the mixture was diluted with DMF and the nanoparticles were collected using a magnet. The final nanoparticles, Fe_3O_4@PVBC, were washed with DMF and THF several times to remove physically adsorbed polymers.

Modification of Fe_3O_4@PVBC nanoparticles with TAEA (Fe_3O_4@PVBC-TAEA)

Fe_3O_4@PVBC nanoparticles of 50 mg were dispersed into 10 mL of DMF in a 25-mL round-bottom flask. Three milliliters of TAEA was added into the suspension while stirring. The mixture was heated to 60 °C and stirred at 600 rpm for 24 h. The final Fe_3O_4@PVBC-TAEA nanoparticles were isolated by a magnet from the solution and washed with DMF, water, and methanol until pH value reached 7. The Fe_3O_4@PVBC-TAEA nanoparticles were dried under vacuum at 50 °C.

Batch Pb(II) adsorption tests

Pb(II) stock solution (1000 mg/L) was prepared by dissolving a suitable amount of lead nitrate (Pb $(NO_3)_2$) in 500 mL ultrapure water. This stock solution was diluted to obtain the desired concentration range of Pb(II). The initial pH adjustment of all solutions was done by adding 0.1 N NaOH or HNO_3 solutions.

Batch-mode adsorption tests generated by CCD were operated on a shaking water bath (Nuve ST30, Turkey) at 250 rpm in 100 mL Erlenmeyer flasks containing 50 mL Pb(II) solution at room temperature. All experiments were carried out under different adsorption conditions including initial pH (2–9), C_0 (10–100 mg/L), adsorbent dosage (5–50 mg/50 mL (100–1000 mg/L)), and contact time (10–120 min). After the adsorption process, the un-adsorbed Pb(II) concentration in filtration solutions was quantified by AAS. The percentage of Pb(II) adsorption and the amount of adsorbed Pb(II) ions were determined from the following equations:

$$Q_e = \frac{(C_0 - C_e)V}{m} \tag{1}$$

$$Pb(II)Adsorption, \% = \frac{(C_0 - C_e)}{C_0} \times 100 \tag{2}$$

where Q_e is the adsorbed amount (mg/g), C_0 and C_e (mg/L) are the initial and final Pb(II) concentration, respectively, V (L) is the aqueous solution volume, and m (g) is the amount of Fe_3O_4@PVBC-TAEA used.

Experimental design by CCD

Optimization is widely described as a means of determining the conditions in which a procedure can give the best possible response. Experimental design can be used to optimize processes and then to create a mathematical model by spreading the individual and interactive effects of the arguments simultaneously across all domains (Sohbatzadeh et al. 2016). The four independent parameters, namely, initial pH (X_1), C_0 (X_2), adsorbent dosage (mg/50 mL) (X_3), and contact time (min) (X_4), were chosen for Pb(II) adsorption (%) which is the dependent parameter (the response). CCD under RSM was applied for modeling and optimizing the relations between the response and the selected parameters. Thirty experimental data sets were designed by CCD to obtain Pb(II) adsorption from aqueous media using the equation $2^k + 2k + 6$ (k is 4 for this study). At central levels of these parameters, six experiments were performed to determine experimental error. These levels (central (*0*), highest (*+ 1*) and lowest (*− 1*)) are given in Table 1. An empirical second-order polynomial model representing system behavior is given as follows:

$$\hat{y}_n = \beta_o + \sum_{i=1}^{4} \beta_i x_i + \sum_{i=1}^{4} \beta_{ii} x_i^2 + \sum_{i=1}^{4} \sum_{j=i+1}^{4} \beta_{ij} x_i x_j \tag{3}$$

where $\hat{y}_n$ is the predicted Pb(II) adsorption (%), X_i and X_j represent the independent parameters, β_0 is the constant value, and β_i, β_{ii}, and β_{ij} are the linear, the second-order, and the dual interaction between parameters, respectively.

Variance analysis (ANOVA) with Design-Expert 7.0 software (test version) was utilized to evaluate the statistical significance of parameters and interaction effects between the response and the process parameters. The accuracy of the quadratic model was evaluated using the value of the determination coefficient (R^2).

Results and discussion

Preparation and surface characterization of the magnetic samples

Scheme 1 presents the synthetic procedure for the preparation of the Fe_3O_4@PVBC-TAEA nanoparticles. First, Fe_3O_4@OA nanoparticles were synthesized via chemical co-precipitation of Fe^{2+}/Fe^{3+} in basic medium in the presence of oleic acid. Then, the Fe_3O_4@CTA nanoparticles were prepared by a simple ligand exchange reaction between OA and CTA. As a result, the Fe_3O_4@CTA nanoparticles could be used as a supporting material for the preparation of a uniform PVBC brush layer through SI-RAFT polymerization in the presence of VBC and AIBN. Subsequently, the PVBC brushes were aminated through a simple displacement reaction between chlorine atoms of PVBC and amine groups of TAEA.

The size and shape of the nanoparticles were determined by TEM analysis. As shown in Fig. 1a, bare Fe_3O_4 nanoparticles had irregular shape with a mean diameter of 12.4 ± 2.1 nm (counted on 120 nanoparticles). The shape and diameter of the nanoparticles did not significantly change after the ligand exchange reaction between CTA and OA (Fig. 1b). As presented in Fig. 1c, a bright layer was observed on the nanoparticles after SI-RAFT polymerization indicating that the polymer layer was successfully grafted on the nanoparticles with a mean thickness of 26.7 ± 3.9 nm (based on 20 randomly selected regions). Note that the presence of thin polymer layer on the nanoparticles is desirable for practical applications to achieve fast kinetics and high adsorption capacity.

XPS analysis was conducted to evaluate chemical characteristics of the nanoparticles for each modification step. XPS wide scan spectra of bare Fe_3O_4@OA (a), Fe_3O_4@CTA (b), Fe_3O_4@PVBC (c), and Fe_3O_4@PVBC-TAEA (d) are shown in Fig. 2. After the ligand exchange reaction between OA and CTA, two new peaks were observed at about 225.1 and 162.6 eV which could be due to S 2s and S 2p, respectively, indicating the attachment of CTA to the nanoparticles. The presence of chlorine peaks at 270.1 eV (Cl 2s) and 199.6 eV (Cl 2p) in the XPS spectrum of Fe_3O_4@PVBC after SI-RAFT polymerization proved the presence of PVBC on the nanoparticles. Furthermore, the iron peaks in the XPS spectrum of Fe_3O_4@PVBC could not be observed due to the thickness of the polymer layer which is larger than the typical X-ray depth length (~ 10 nm). The disappearance of chlorine peaks and the appearance of nitrogen peaks at about 400.1 eV in the XPS spectrum of Fe_3O_4@PVBC-TAEA clearly showed the successful post-modification of PVBC brushes with TAEA.

VSM analysis was carried out to evaluate the magnetic properties of the nanoparticles. The hysteresis loops in Fig. 3 showed that for all nanoparticles, the loops were symmetrical and both coercivity and remanence of the magnetic nanoparticles were zero implying the nanoparticles had superparamagnetic behavior at room temperature. The saturation magnetization values of the samples were 63.3, 60.7, and 26.7 emu/g for bare Fe_3O_4, Fe_3O_4@CTA, and Fe_3O_4@PVBC-TAEA, respectively. The decrease in magnetization after polymerization could be attributed to the presence of a polymer layer on the nanoparticles. Moreover, the saturation magnetization value of Fe_3O_4@PVBC-TAEA is sufficient for magnetic separation of heavy metal ions (Khayat Sarkar and Khayat Sarkar 2013; Santhosh et al. 2017; Xia et al. 2014).

Experimental and statistical analysis

The maximum Pb(II) adsorption and the influences of the studied independent parameters on the Pb(II) adsorption were examined with the experiments designed in RSM according to CCD. The experimental design matrix obtained by CCD and the relevant response data are given in Table 2. The relationship between the selected parameters and Pb(II) adsorption are shown in the following quadratic model equations:

$$\begin{aligned} Pb(II)\,adsorption,\%(real,uncoded) = {} & -8.62555 + 10.47580\,[pH] + 0.76254\,[C_0] + 1.71335\,[Ads.dosage] \\ & +0.77100\,[Contact\quad time] + 0.017621\,[pH][C_0] + 0.018651\,[pH][Ads.dosage] + 4.44610E{-}003\,[pH][Contact\quad time] \\ & -4.13309E{-}003\,[C_0][Ads.dosage] - 1.73864E{-}003\,[C_0][Contact\quad time] - 3.89818E{-}003\,[Ads.dosage][Contact\quad time] \\ & -0.87644\,[pH]^2 - 8.11303E{-}003\,[C_0]^2 - 0.020895\,[Ads.dosage]^2 - 3.46409E{-}003\,[Contact\quad time]^2 \end{aligned} \tag{4}$$

$$\begin{aligned} Pb(II)adsorption,\%(coded) = {} & +96.98 + 9.12[X_1] - 11.68[X_2] + 4.19[X_3] + 7.83[X_4] + 2.78[X_1X_2] \\ & +1.47[X_1X_3] + 0.86[X_1X_4] - 4.18[X_2X_3] - 4.30[X_2X_4] - 4.82[X_3X_4] - 10.74[X_1]^2 - 16.43[X_2]^2 \\ & -10.58[X_3]^2 - 10.48[X_4]^2 \end{aligned} \tag{5}$$

ANOVA was completed to verify the statistical significance of interactive influences of each parameter and their interactions in the obtained quadratic model (Table 3). R^2 of the quadratic model was found to be 0.93. As a result, it can be said that the quadratic model equation has considerably credible. Moreover, the low value of p indicated that the variations

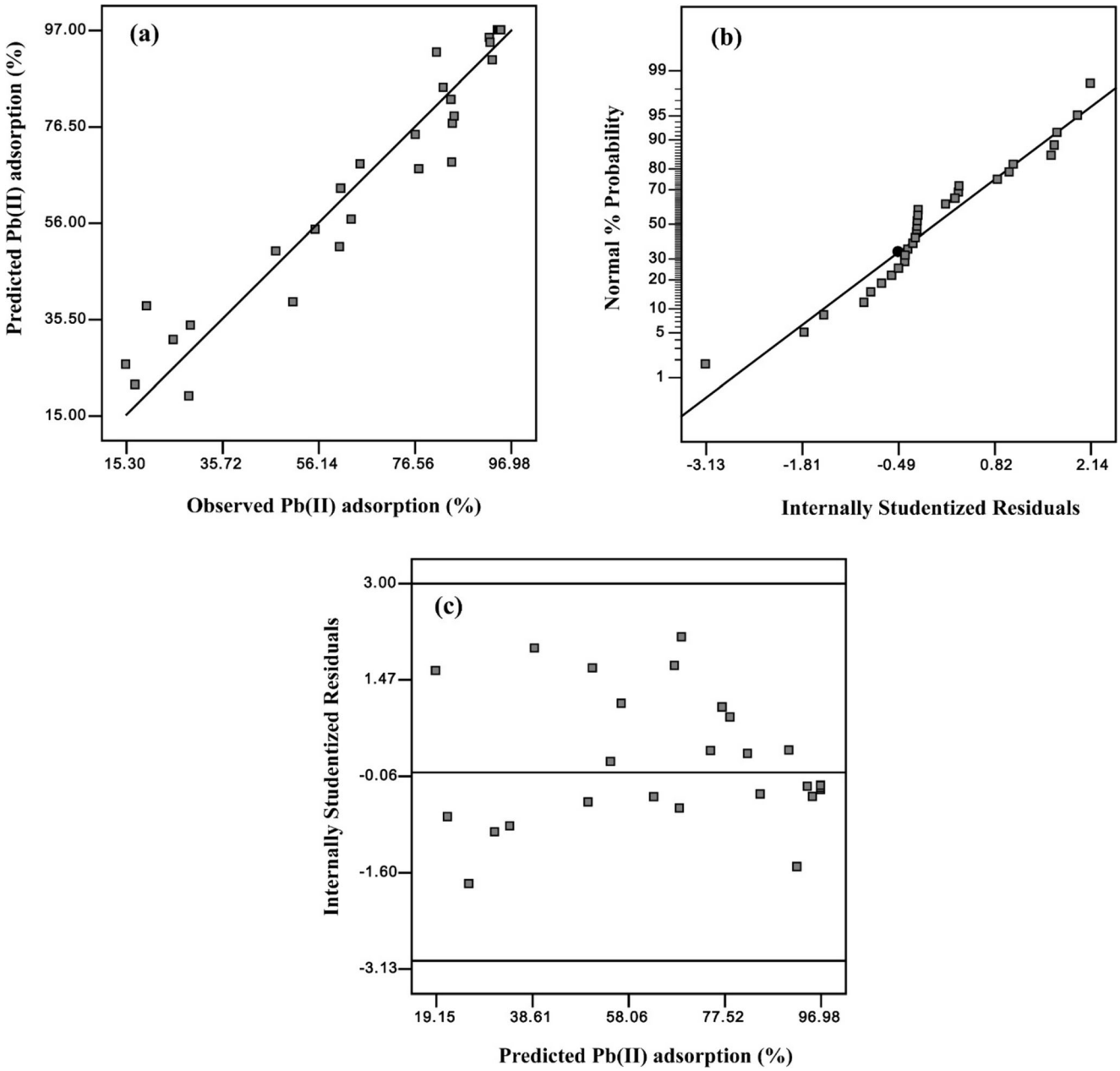

Fig. 4 **a** The observed versus predicted values of the response. **b** Pb(II) adsorption residuals versus normal % probability. **c** Studentized residuals vs. the predicted data

among model parameters could be explained by the quadratic model equation. As seen from Table 3, the main effects of initial pH, C_0, and contact time are highly significant due to the low p values. Additionally, the quadratic effect of C_0 is also statically significant. On the other hand, the other model terms appear to be insignificant, but they have little effect on the response. Therefore, the linear, quadratic, and interaction effects of all independent parameters are considered in the optimization studies.

The relationship between the observed and predicted values is displayed in Fig. 4a. It clearly indicates that the observed values were in good agreement with the predicted values. The normal percentage probability plot vs. residuals is given in Fig. 4b. The points on the plot were normally distributed on a straight line, confirming that the congruity of the model for Pb(II) adsorption is fairly satisfactory. The residuals of the predicted values were randomly scattered on the plot (Fig. 4c), indicating that the harmony between the observed and predicted values coheres very well with each other for Pb(II) adsorption.

The initial pH of the aqueous solution is a major parameter affecting the adsorption processes. The initial pH range between 2 and 9 was studied to analyze the influence of initial pH on Pb(II) adsorption from aqueous media. Pb(II)

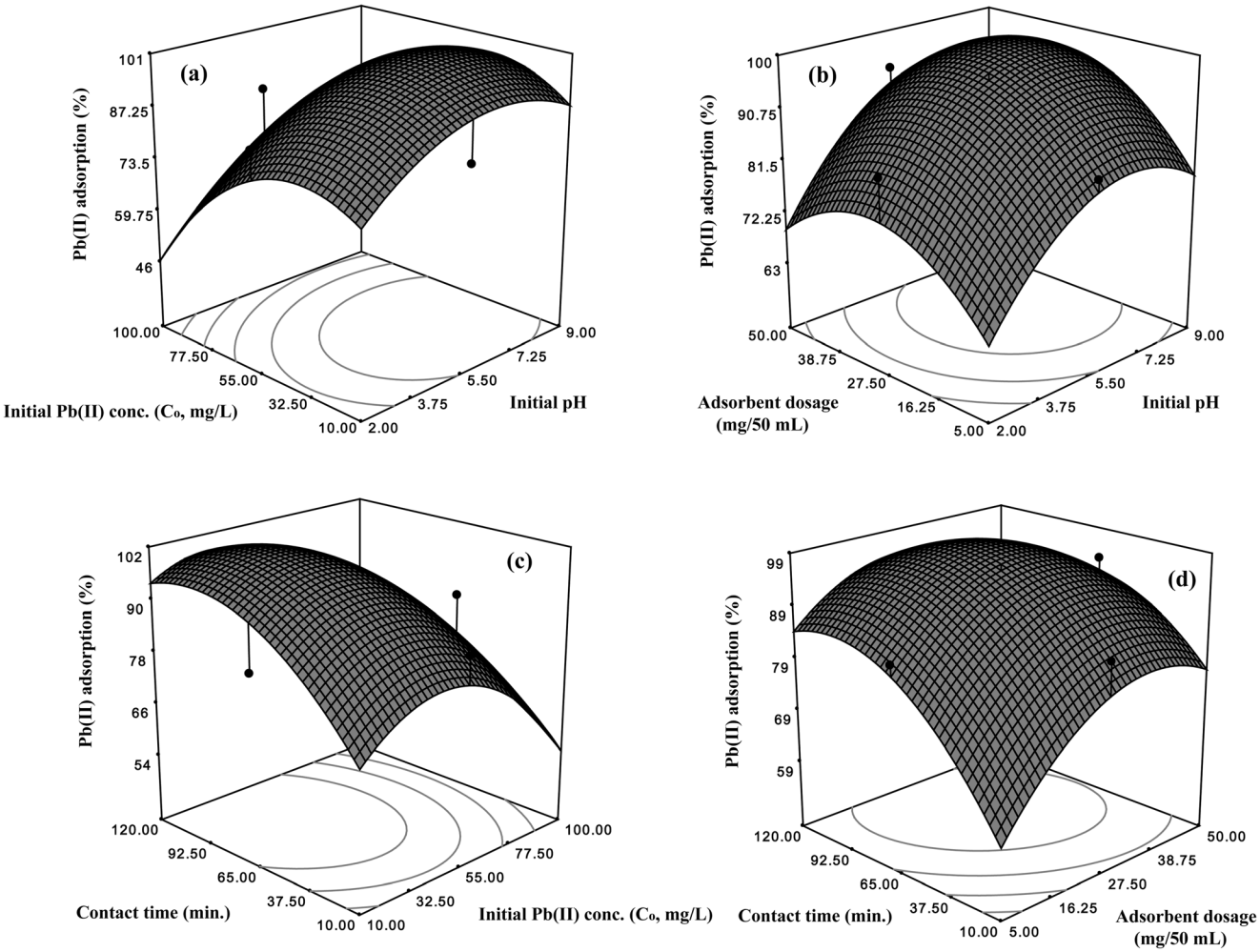

Fig. 5 Response surface plots for Pb(II) adsorption depending on **a** C_0 and initial pH (at adsorbent dosage = 27.5 mg and contact time = 65 min), **b** adsorbent dosage and initial pH (at C_0 = 55 mg/L and contact time = 65 min), **c** contact time and C_0 (at adsorbent dosage = 27.5 mg and initial pH = 5.5), and **d** contact time and adsorbent dosage (at initial pH = 5.5 and C_0 = 55 mg/L)

adsorption firstly increased along with the increment of initial pH range from 2 to 6, then, at higher initial pH than 6, there was a reduction in Pb(II) adsorption (Fig. 5a, b). The surface of iron oxides is enveloped by hydroxyl (-OH) groups in aqueous systems. The iron oxide surfaces can easily protonate or deprotonate in acidic and basic ambient conditions, respectively, depending on initial pH. In this respect, Rajput et al. (2016) reported that the surface species of iron oxide are

Table 4 Comparison of different adsorbents for the uptake of Pb(II)

Adsorbent	C_0 (mg/L)	Adsorbent dosage (mg/50 mL)	Pb(II) adsorption (%)	Reference
Sargassum ilicifolium	200	10	19.5	Tabaraki et al. (2014)
Pumice	84.30	500	88.49	Şahan and Öztürk (2014)
Bentonite immobilized alginate grafted by polyacrylonitrile (PAB) nanocomposite	55	30	96.65	Ahmad and Hasan (2016)
Magnetic magnetite (Fe_3O_4) nanoparticle	100	2.5	91	Rajput et al. (2016)
Triethylene-tetramine grafted magnetic chitosan	200	25	92.66	Kuang et al. (2013)
Fe_3O_4/talc nanocomposite	270	240	91.35	Kalantari et al. (2014)
Fe_3O_4/montmorillonite nanocomposite	510.16	120	89.72	Kalantari et al. (2015)
Fe_3O_4@PVBC-TAEA	46.51	17.41	97.07	This study

Table 5 The parameters of kinetic models for Pb(II) adsorption

Pseudo-first-order kinetic model	Pseudo-second-order kinetic model	Weber-Morris model
q_e 46.92 mg/g	q_e 129.87	C 78.83
k_1 0.035	k_2 0.0019	k_{id} 6.07
R^2 0.98	R^2 0.99	R^2 0.99

positively charged (Fe^{2+}, $FeOH^+$) in acidic solution, while these species are generally in $Fe(OH)_2^0$, and Fe $(OH)_3^-$ form in basic solutions. Furthermore, the amine groups which varied with initial pH cause the protonation degree of the Fe_3O_4@PVBC-TAEA surface to increase and decrease in acidic and basic solutions, respectively (Shen et al. 2015). Under low initial pH conditions, the reduction of Pb(II) adsorption may be due to the electrostatic repulsion between Pb(II) ions and the surface charges of Fe_3O_4@PVBC-TAEA. With the increase in initial pH value, the removal percentage of Pb(II) increased depending on the increment of the degree of deprotonation of the surface and loss of repulsions between the adsorbent and metal ions. However, it is well-known that the dominant species of Pb(II) is Pb $(OH)_2$ when initial pH is greater than 6 (Bagbi et al. 2017). Moreover, the effect of the point of zero charge (pH_{pzc}) value of the adsorbent on the Pb(II) adsorption was investigated. The pH_{pzc} value of the Fe_3O_4@PVBC-TAEA was determined as 4.94 according to the previously used method in the literature (Fig. S1) (Mall et al. 2006). The total charge of the Fe_3O_4@PVBC-TAEA surface is equal to zero at pH 4.94, indicating that the surface of the adsorbent is negatively charged at pH > 4.94 and positively charged at pH < 4.94. Therefore, the removal percentage of Pb(II) increased at higher pH values than pH_{pzc} because of the attractive interaction, while it decreased at lower pH values than pH_{pzc} because of electrostatic repulsion. Therefore, it may be said that Pb(II) adsorption reached the maximum at about pH 6. Such observations have also been reported by various researchers (El-Kassas et al. 2016; Huang et al. 2015; Jiang et al. 2017; Rajput et al. 2017; Shen et al. 2015; Şahan and Öztürk 2014).

The effect of C_0 on Pb(II) adsorption was examined in the range between 10 and 100 mg/L. From three-dimensional response surface plots (Fig. 5a, c) related to C_0, it can be concluded that Pb(II) adsorption increases rapidly until 50 mg/L. At the next level, a reduction in uptake of Pb(II) was recognized. This reduction in Pb(II) adsorption is attributed to a decrease in the accessibility of the active adsorption sites on the Fe_3O_4@PVBC-TAEA surface. In other words, the free sites on the surface of the adsorbent were filled with Pb(II) ions and reached a state of equilibrium. In addition to this, increasing C_0 supplied less driving force to cope with mass transfer resistance between solid and aqueous phases (Afshar et al. 2016; Ahmad and Hasan 2016; Gurgel and Gil 2009; Kalantari et al. 2015). When all the results are considered, Pb(II) adsorption reaches an equilibrium state in the range of 45–50 mg/L, attributed to the fact that all sites were saturated with Pb(II) ions.

The influence of the adsorbent dosage on removal percentage of Pb(II) was investigated by using different adsorbent dosages varying from 5 to 50 mg/50 mL (100–1000 mg/L). Pb(II) adsorption increased with a step-up in the adsorbent dosage in the range of 5 to 20 mg/50 mL (100 to 400 mg/L) (Fig. 5b, d). The increase in removal of Pb(II) adsorption is due more surface area being present depending on increased active sites on Fe_3O_4@PVBC-TAEA (Afshar et al. 2016; Kalantari et al. 2015; Kuang et al. 2013; Yılmaz et al. 2017). At later levels, Pb(II) adsorption remains unchanged. The effect of contact time on Pb(II) adsorption was regulated by dissimilar contact time ranging from 10 to 120 min. From Fig. 5c, d, Pb(II) adsorption on Fe_3O_4@PVBC-TAEA increased by increasing the contact time from 10 to 100–110 min because of the abundance of free sites on the adsorbent up to the equilibrium stage. After the equilibrium stage, Pb(II) adsorption remains unchanged (Ahmad and Hasan 2016; Anna et al. 2015; Gurgel and Gil 2009).

Numerical analysis of Pb(II) adsorption for optimization

Numerical optimization based on CCD was performed to appoint the maximum Pb(II) adsorption and the optimal conditions of parameters. The maximum response was scanned by

Table 6 Constants of the used isotherm models for Pb(II) adsorption

Model	Parameters			
Langmuir isotherm	q_{max}	K_L	R_L	R^2
	200 mg/g	1.25 L/mg	0.0099	0.99
Freundlich isotherm	n	K_f		R^2
	5.22	119.98		0.97
Dubinin-Radushkevich isotherm	q_m	B_D	E	R^2
	178.07 mg/g	2.00E − 07 mol^2/J^2	1.28 kJ/mol	0.93

Table 7 The values of thermodynamic parameters

T (K)	293	303	313	323
$\ln K_d$	2.61	2.53	2.36	2.25
$\Delta G°$ (kJ/mol)	− 6.40	− 6.28	− 6.16	− 6.04
$\Delta H°$ (kJ/mol)	− 9.89			
$\Delta S°$ (J/mol K)	− 11.91			

Table 8 The composition of the multi-metal systems

Samples	The heavy metal concentrations (mg/L)		
	Cd(II)	Pb(II)	Ni(II)
Battery industry	0.05	5.16	4.78
Paint-adhesive industry	0.27	9.53	1.48
Textile industry	0.31	3.17	1.05

setting the values of initial pH, C_0, adsorbent dosage, and contact time at "in range" level. Among the solutions produced by the software, the best was chosen for optimal adsorption conditions. Numerical optimization gave the optimum points for independent parameters as initial pH of 5.88, C_0 of 46.51 mg/L, adsorbent dose of 17.41 mg/50 mL (348.2 mg/L), and contact time of 108.21 min. At these conditions, the maximum removal efficiency and the adsorption capacity of Pb(II) were 97.07 and 129.65 mg/g, respectively. A number of tests were completed to confirm the predicted values in the quadratic model under the same conditions. Pb(II) adsorption was experimentally found to be 96.65%, indicating that the high trustworthiness of the model for Pb(II) adsorption onto Fe_3O_4@PVBC-TAEA. Consequently, RSM is an effective and reliable tool for identification of optimal conditions of adsorption parameters for the removal of heavy metals.

A comparison of the adsorbent in this study with other adsorbents reported earlier for Pb(II) adsorption is summarized in Table 4. The results showed that the Fe_3O_4@PVBC-TAEA exhibited higher removal efficiency. This is attributed to the abundance of existing sites on the surface of the adsorbent. These nanoparticles with high potency are promising for Pb(II) adsorption from aqueous media.

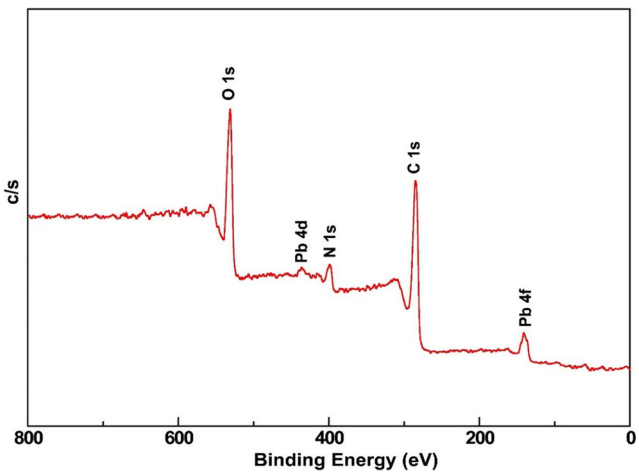

Fig. 6 XPS wide scan spectrum of Fe_3O_4@PVBC-TAEA nanoparticles after Pb(II) adsorption

Kinetic, isotherm, and thermodynamic studies

The adsorption kinetic models such as the pseudo-first-order (Eq. (S1)) (Lagergren 1898), the pseudo-second-order (Eq. (S2)) (Ho and McKay 1999), and Weber-Morris (Eq. (S3)) (Weber and Morris 1963) were used to evaluate the kinetic behavior of the adsorption system as a function of time. The values of the studied kinetic model parameters were calculated through the linear plots, as seen in Fig. S2. The obtained results are presented in Table 5. The pseudo-second-order model fit well to Pb(II) adsorption data due to high R^2, indicating that the pseudo-second-order model is more satisfactory. Additionally, the difference between the experimentally calculated q_e value (129.65 mg/g) and the q_e value (129.87 mg/g) calculated by the pseudo-second-order model equation is rather small; namely these values comply with each other. The transfer mechanism of Pb(II) ions between the solution and adsorbent was evaluated by Weber-Morris model equation. From this model, it can be said that intraparticle diffusion is only available in the adsorption system when a straight line passes from the origin of the model. On the contrary, in the present study, the experimental data showed that both intraparticle and film diffusion are effective in the determination of the Pb(II) adsorption rate due to the intercept being greater than zero (Afshar et al. 2016; Grewal and Kaur 2017; Song et al. 2018; Taty-Costodes et al. 2003).

The adsorption isotherms have a major role in understanding the interaction of adsorbate with the adsorbent. The well-known isotherm models including Langmuir (Eq. (S4)) (Langmuir 1918), Freundlich (Eq. (S5)) (Freundlich 1906), and Dubinin-Radushkevich (D-R) (Eq. (S6)) (Dubinin and Radushkevich 1947) were fitted to the adsorption data. The results indicated that both the Langmuir and Freundlich models are more consistent with the obtained adsorption data (Fig. S3 and Table 6). It can be said that the adsorption sites have monolayer adsorption and homogenous distribution at high Pb(II) concentrations, while they have multilayer adsorption and heterogeneous distribution at low Pb(II) concentrations (Grewal and Kaur 2017; Rajput et al. 2016). R_L value (Eq. (S7)) is expected to be between 0 and 1. In the present study, this value was found to be 0.0099, indicating that the removal of Pb(II) appears to be a favorable adsorption. Moreover, the adsorption process is favorable considering

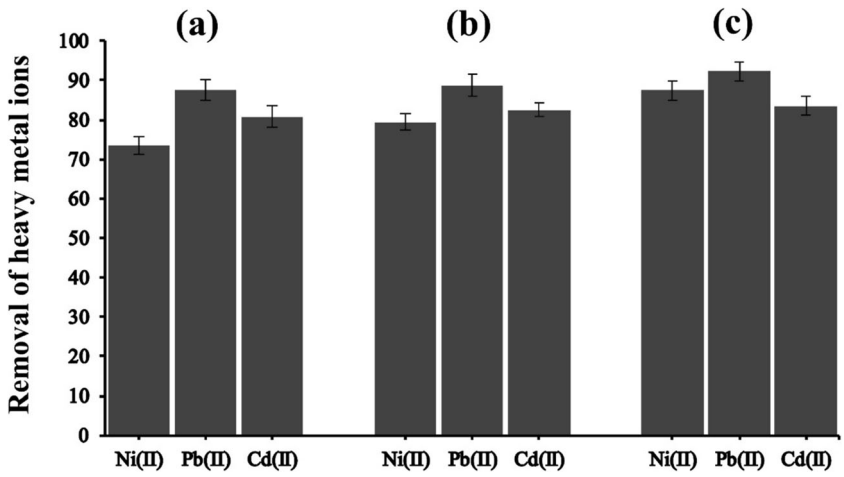

Fig. 7 Removal of heavy metal ions from multi-metal systems: (a) battery, (b) paint-adhesive, (c) textile industry

that the value of n is higher than 1. E (kJ/mol) is the adsorption energy and was calculated from Eq. (S8). The value of E in this work is found to be 1.58, indicating that the adsorption is a physical adsorption process (Şahan and Öztürk 2014; Tan et al. 2012).

The thermodynamic analysis was performed to investigate the thermodynamic behavior of the adsorption process under different temperatures (20, 30, 40, and 50 °C). The thermodynamic parameters such as enthalpy change ($\Delta H°$), Gibbs free energy change ($\Delta G°$), and entropy change ($\Delta S°$) were measured to determine the nature of adsorption. These thermodynamic parameters were computed from Eq. S9 to S12. The values of the thermodynamic parameters were obtained by plotting $\ln K_d$ against $1/T$ (Fig. S4). As seen in Table 7, the negative $\Delta G°$ value indicated that Pb(II) adsorption is a spontaneous process and applicable in nature. Additionally, the value of $\Delta G°$ increased with increasing temperature, resulting in the adsorption system having more spontaneity and feasibility at low temperature (Devi et al. 2017; Kuang et al. 2013). The negative value of $\Delta S°$ means that the randomness at the solid/solution interfaces decreases during the adsorption process. The calculated negative value of $\Delta H°$ shows that the Pb(II) adsorption onto Fe_3O_4@PVBC-TAEA is exothermic in nature (Grewal and Kaur 2017; Haiyan et al. 2016; Kuang et al. 2013).

The adsorption mechanism of Pb(II) onto Fe_3O_4@PVBC-TAEA was also evaluated by XPS (Fig. 6). The signals of Pb 4f and Pb 4d were observed after adsorption at about 140.1 and 435.9 eV, respectively. Moreover, the peak at 400.1 eV attributed to N 1s in Fig. 2d was shifted to lower binding energy of 398.9 eV after adsorption of Pb(II). These results indicated amine groups of TAEA are binding sites for Pb(II) (Luo et al. 2017). Generally, Pb(II) ions can coordinate with four organic ligands. In this case, it can be concluded that Pb(II) coordinates with four amine groups of TAEA containing two adjacent polymer brushes.

Application of the Fe_3O_4@PVBC-TAEA to the multi-metal systems

The Fe_3O_4@PVBC-TAEA was applied to the multi-metal systems to check the removal of different heavy metal ions. The multi-metal compositions used for the experiments are

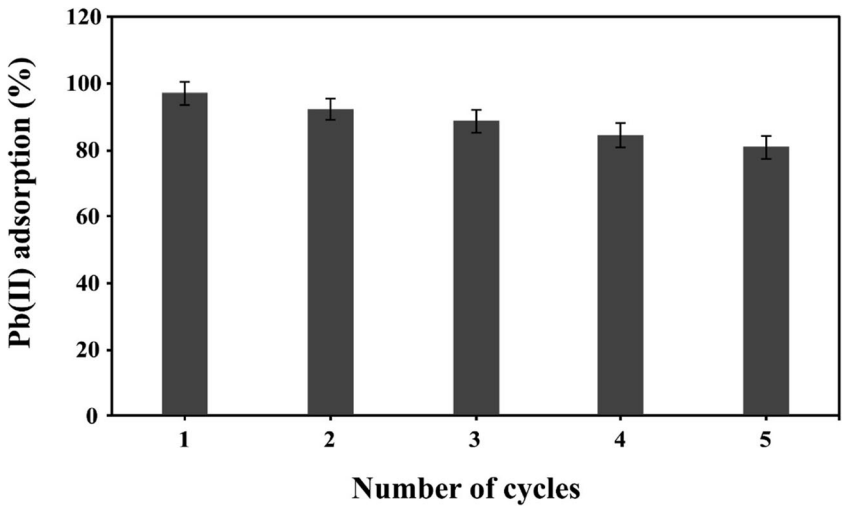

Fig. 8 The effect of regeneration of Fe_3O_4@PVBC-TAEA on the Pb(II) removal efficiency

summarized in Table 8 (Chand et al. 2015). These samples including multi-metal ions were prepared artificially under laboratory conditions. The adsorption experiments for the prepared multi-metal solutions were performed at predetermined optimum conditions. According to the obtained results (Fig. 7), the removal percentages of Pb(II) ions were found to be 87.79, 85.95, and 89.66% for the battery, paint-adhesive, and textile industry, in their given order. Furthermore, the results indicate clearly that the performance of the Fe_3O_4@PVBC-TAEA for Pb(II) ions is higher than for other heavy metal ions. It can be concluded that the Fe_3O_4@PVBC-TAEA is an effective adsorbent with high selectivity for Pb(II).

Regeneration and stability of Fe_3O_4@PVBC-TAEA

The regeneration of the adsorbent is significant for stability and re-usability. Thus, five adsorption–desorption cycles were performed for this purpose. The regeneration studies were carried out under the optimal conditions obtained with the numerical analysis. The regeneration process was performed using HNO_3. The adsorbent loaded with Pb(II) ions was magnetically separated from aqueous solution and treated with 0.5 M HNO_3 (Afshar et al. 2016). This procedure was repeated consecutively. From Fig. 8, the percentage of Pb(II) adsorption diminished with increasing cycle number, but the reduction rate in the removal efficiency is not very high and is satisfactory. The results indicated that Fe_3O_4@PVBC-TAEA has important potential in terms of re-usability and stability. It can be said that the adsorbent could be successfully applied for the removal of Pb(II) from aqueous environments after the regeneration steps.

Conclusions

In conclusion, the Fe_3O_4@PVBC was successfully synthesized via SI-RAFT polymerization and subsequently modified with TAEA. The presence of amine groups on the PVBC brushes was verified by XPS. TEM analysis also showed a polymer layer on the nanoparticles. VSM analysis indicated that the aminated PVBC brush grafted magnetic nanoparticles showed superparamagnetic behavior at room temperature. RSM was successfully utilized to find the optimization of the uptake of Pb(II) adsorption from aqueous environment by the synthesized Fe_3O_4@PVBC-TAEA. With respect to numerical analysis, the optimum adsorption conditions obtained by the quadratic model for the maximum Pb(II) adsorption onto Fe_3O_4@PVBC-TAEA were determined to be 5.88, 46.51 mg/L, 17.41 mg/50 mL (348.2 mg/L), and 108.21 min for initial pH, C_0, adsorbent dosage, and contact time, in their given order. From the determined optimal conditions, the maximum removal efficiency and adsorption capacity were found to be 97.07% and 129.65 mg/g, respectively. The obtained kinetic results demonstrated that the adsorption process was in accordance with the pseudo-second-order and Weber-Morris models. Adsorption isotherm studies showed that the Langmuir and Freundlich isotherm models fit better than the D-R. Moreover, the thermodynamic studies revealed that the adsorption mechanism was exothermic, spontaneous, and applicable. Consequently, it can be stated that Fe_3O_4@PVBC-TAEA is an efficient adsorbent with high selectivity for heavy metal ions removal such as Pb(II) from aqueous environment in the future.

Acknowledgments The authors thank Prof. Dr. Zekiye Suludere for TEM analysis.

Compliance with ethical standards

Conflict of interest The authors declare that they have no conflict of interest.

References

Afshar A, Sadjadi SAS, Mollahosseini A, Eskandarian MR (2016) Polypyrrole-polyaniline/Fe_3O_4 magnetic nanocomposite for the removal of Pb(II) from aqueous solution. Korean J Chem Eng 33:669–677

Ahmad R, Hasan I (2016) Optimization of the adsorption of Pb(II) from aqueous solution onto PAB nanocomposite using response surface methodology. Environ Nanotechnol Monit Manage 6:116–129

Ahmadi A, Heidarzadeh S, Mokhtari AR, Darezereshki E, Harouni HA (2014) Optimization of heavy metal removal from aqueous solutions by maghemite (γ-Fe_2O_3) nanoparticles using response surface methodology. J Geochem Explor 147:151–158

Anna B, Kleopas M, Constantine S, Anestis F, Maria B (2015) Adsorption of Cd(II), Cu(II), Ni(II) and Pb(II) onto natural bentonite: study in mono- and multi-metal systems. Environ Earth Sci 73:5435–5444

Antonopoulou M, Chondrodimou I, Bairamis F, Giannakas A, Konstantinou I (2017) Photocatalytic reduction of Cr(VI) by char/TiO_2 composite photocatalyst: optimization and modeling using the response surface methodology (RSM). Environ Sci Pollut Res 24:1063–1072

Bagbi Y, Sarswat A, Mohan D, Pandey A, Solanki PR (2017) Lead and chromium adsorption from water using L-cysteine functionalized magnetite (Fe_3O_4) nanoparticles. Sci Rep UK 7:7672–7686

Banaei A, Vojoudi H, Karimi S, Bahar S, Pourbasheer E (2015) Synthesis and characterization of new modified silica coated magnetite nanoparticles with bisaldehyde as selective adsorbents of Ag(I) from aqueous samples. RSC Adv 5:83304–83313

Bezerra MA, Santelli RE, Oliveira EP, Villar LS, Escaleira LA (2008) Response surface methodology (RSM) as a tool for optimization in analytical chemistry. Talanta 76:965–977

Calugaru IL, Neculita CM, Genty T, Zagury GJ (2019) Removal efficiency of As(V) and Sb(III) in contaminated neutral drainage by Fe-loaded biochar. Environ Sci Pollut Res 26:9322–9332

Chand P, Bafana A, Pakade YB (2015) Xanthate modified apple pomace as an adsorbent for removal of Cd(II), Ni(II) and Pb(II), and its application to real industrial wastewater. Int Biodeterior Biodegrad 97:60–66

Deng S, Zheng YQ, Xu FJ, Wang B, Huang J, Yu G (2012) Highly efficient sorption of perfluorooctane sulfonate and perfluorooctanoate on a quaternized cotton prepared by atom transfer radical polymerization. Chem Eng J 193-194:154–160

Devi V, Selvaraj M, Selvam P, Kumar AA, Sankar S, Dinakaran K (2017) Preparation and characterization of CNSR functionalized Fe_3O_4 magnetic nanoparticles: an efficient adsorbent for the removal of cadmium ion from water. J Environ Chem Eng 5:4539–4546

Djouani F, Herbst F, Chehimi MM, Benzarti K (2011) Synthesis, characterization and reinforcing properties of novel, reactive clay/poly (glycidyl methacrylate) nanocomposites. Constr Build Mater 25: 424–431

Dubinin M, Radushkevich L (1947) Equation of the characteristic curve of activated charcoal. Proc Acad Sci Phys Chem Sec USSR 55:331–333

Elkady M, Hassan H, Hashim A (2016) Immobilization of magnetic nanoparticles onto amine-modified nano-silica gel for copper ions remediation. Materials 9:460–483

El-Kassas HY, Aly-Eldeen MA, Gharib SM (2016) Green synthesis of iron oxide (Fe_3O_4) nanoparticles using two selected brown seaweeds: characterization and application for lead bioremediation. Acta Ocenol Sin 35:89–98

Freundlich H (1906) Over the adsorption in solution. J Phys Chem 57: 385–470

Grewal JK, Kaur M (2017) Effect of core-shell reversal on the structural, magnetic and adsorptive properties of Fe_2O_3-GO nanocomposites. Ceram Int 43:16611–16621

Gurgel LVA, Gil LF (2009) Adsorption of Cu(II), Cd(II), and Pb(II) from aqueous single metal solutions by succinylated mercerized cellulose modified with triethylenetetramine. Carbohyd Polym 77:142–149

Haiyan J, Qiuxiang Z, Ying Z (2016) Removal of Cd(II) and Pb(II) from aqueous solutions by modified polyvinyl alcohol. Desalin Water Treat 57:6452–6462

Ho YS, McKay G (1999) Pseudo-second order model for sorption processes. Process Biochem 34:451–465

Hosseinzadeh H, Pashaei S, Hosseinzadeh S, Khodaparast Z, Ramin S, Saadat Y (2018) Preparation of novel multi-walled carbon nanotubes nanocomposite adsorbent via RAFT technique for the adsorption of toxic copper ions. Sci Total Environ 640-641:303–314

Huang L, Zhou Y, Guo X, Chen Z (2015) Simultaneous removal of 2,4-dichlorophenol and Pb(II) from aqueous solution using organoclays: isotherm, kinetics and mechanism. J Ind Eng Chem 22:280–287

Imamoglu M, Tekir O (2008) Removal of copper(II) and lead(II) ions from aqueous solutions by adsorption on activated carbon from a new precursor hazelnut husks. Desalination 228:108–113

Jiang H, Zhang Y, Chen R, Sun M, Tong H, Xu J (2017) Preparation of ion imprinted magnetic Fe_3O_4 nanoparticles for selective remediation of Pb(II). J Taiwan Inst Chem Eng 80:184–191

Kalantari K, Ahmad M, Masoumi H, Shameli K, Basri M, Khandanlou R (2014) Rapid adsorption of heavy metals by Fe_3O_4/talc nanocomposite and optimization study using response surface methodology. Int J Mol Sci 15:12913–12927

Kalantari K, Ahmad MB, Fard Masoumi HR, Shameli K, Basri M, Khandanlou R (2015) Rapid and high capacity adsorption of heavy metals by Fe_3O_4/montmorillonite nanocomposite using response surface methodology: preparation, characterization, optimization, equilibrium isotherms, and adsorption kinetics study. J Taiwan Inst Chem Eng 49:192–198

Khayat Sarkar Z, Khayat Sarkar F (2013) Selective removal of lead(II) ion from wastewater using superparamagnetic monodispersed iron oxide (Fe_3O_4) nanoparticles as a effective adsorbent. Int J Nanosci Ser 9:109–114

Kuang S-P, Wang Z-Z, Liu J, Wu Z-C (2013) Preparation of triethylenetetramine grafted magnetic chitosan for adsorption of Pb(II) ion from aqueous solutions. J Hazard Mater 260:210–219

Kumari M, Pittman CU, Mohan D (2015) Heavy metals [chromium(VI) and lead(II)] removal from water using mesoporous magnetite (Fe_3O_4) nanospheres. J Colloid Interface Sci 442:120–132

Lagergren S (1898) Zur theorie der sogenannten adsorption geloster stoffe. K Sven Vetensk Handl 24:1–39

Langmuir I (1918) The adsorption of gases on plane surfaces of glass, mica and platinum. J Am Chem Soc 40:1361–1403

Liu X, Shi X, Wang H, Zhang H (2014) Atom transfer radical polymerization of diverse functional SBA-15 for selective separation of proteins. Microporous Mesoporous Mater 200:165–173

Luo X, Yu H, Xi Y, Fang L, Liu L, Luo J (2017) Selective removal Pb(II) ions form wastewater using Pb(II) ion-imprinted polymers with bicomponent polymer brushes. RSC Adv 7:25811–25820

Mall ID, Srivastava VC, Kumar GVA, Mishra IM (2006) Characterization and utilization of mesoporous fertilizer plant waste carbon for adsorptive removal of dyes from aqueous solution. Colloid Surf A 278:175–187

Melnyk IV, Pogorilyi RP, Zub YL, Vaclavikova M, Gdula K, Dąbrowski A, Seisenbaeva GA, Kessler VG (2018) Protection of thiol groups on the surface of magnetic adsorbents and their application for wastewater treatment. Sci Rep UK 8:8592–8604

Naiya TK, Bhattacharya AK, Das SK (2009) Adsorption of Cd(II) and Pb(II) from aqueous solutions on activated alumina. J Colloid Interface Sci 333:14–26

Naseem R, Tahir SS (2001) Removal of Pb(II) from aqueous/acidic solutions by using bentonite as an adsorbent. Water Res 35:3982–3986

Nikraftar N, Ghorbani F (2016) Adsorption of As(V) using modified magnetic nanoparticles with ascorbic acid: optimization by response surface methodology. Water Air Soil Pollut 227:178–195

Rajput S, Pittman CU, Mohan D (2016) Magnetic magnetite (Fe_3O_4) nanoparticle synthesis and applications for lead (Pb^{2+}) and chromium (Cr^{6+}) removal from water. J Colloid Interface Sci 468:334–346

Rajput S, Singh LP, Pittman CU, Mohan D (2017) Lead (Pb^{2+}) and copper (Cu^{2+}) remediation from water using superparamagnetic maghemite (γ-Fe_2O_3) nanoparticles synthesized by flame spray pyrolysis (FSP). J Colloid Interface Sci 492:176–190

Sadeghi S, Azhdari H, Arabi H, Moghaddam AZ (2012) Surface modified magnetic Fe_3O_4 nanoparticles as a selective sorbent for solid phase extraction of uranyl ions from water samples. J Hazard Mater 215-216:208–216

Şahan T, Öztürk D (2014) Investigation of Pb(II) adsorption onto pumice samples: application of optimization method based on fractional factorial design and response surface methodology. Clean Technol Environ 16:819–831

Şahan T, Ceylan H, Şahiner N, Aktaş N (2010) Optimization of removal conditions of copper ions from aqueous solutions by *Trametes versicolor*. Bioresour Technol 101:4520–4526

Şahan T, Erol F, Yılmaz Ş (2018) Mercury(II) adsorption by a novel adsorbent mercapto-modified bentonite using ICP-OES and use of response surface methodology for optimization. Microchem J 138:360–368

Sánchez J, Espinosa C, Pooch F, Tenhu H, Pizarro GC, Oyarzún DP (2018) Poly(N,N-dimethylaminoethyl methacrylate) for removing chromium(VI) through polymer-enhanced ultrafiltration technique. React Funct Polym 127:67–73

Santhosh C, Nivetha R, Kollu P, Srivastava V, Sillanpää M, Grace AN, Bhatnagar A (2017) Removal of cationic and anionic heavy metals from water by 1D and 2D-carbon structures decorated with magnetic nanoparticles. Sci Rep UK 7:14107–14117

Sarı A, Tuzen M (2009) Kinetic and equilibrium studies of biosorption of Pb(II) and Cd(II) from aqueous solution by macrofungus (*Amanita rubescens*) biomass. J Hazard Mater 164:1004–1011

Shen H-Y, Chen Z-X, Li Z-H, Hu M-Q, Dong X-Y, Xia Q-H (2015) Controlled synthesis of 2,4,6-trichlorophenol-imprinted amino-functionalized nano-Fe_3O_4-polymer magnetic composite for highly selective adsorption. Colloid Surf A 481:439–450

Sohbatzadeh H, Keshtkar AR, Safdari J, Fatemi F (2016) U(VI) biosorption by bi-functionalized *Pseudomonas putida* @ chitosan bead: modeling and optimization using RSM. Int J Biol Macromol 89:647–658

Song T, Yu C, He X, Lin J, Liu Z, Yang X, Zhang Y, Huang Y, Tang C (2018) Synthesis of magnetically separable porous BN microrods@Fe_3O_4 nanocomposites for Pb(II) adsorption. Colloid Surf A 537:508–515

Stenzel MH, Davis TP (2002) Star polymer synthesis using trithiocarbonate functional β-cyclodextrin cores (reversible addition–fragmentation chain-transfer polymerization). J Polym Sci A1 40:4498–4512

Sun Y, Ding X, Zheng Z, Cheng X, Hu X, Peng Y (2006) Magnetic separation of polymer hybrid iron oxide nanoparticles triggered by temperature. Chem Commun 26:2765–2767

Tabaraki R, Nateghi A, Ahmady-Asbchin S (2014) Biosorption of lead (II) ions on *Sargassum ilicifolium*: application of response surface methodology. Int Biodeterior Biodegradation 93:145–152

Tan Y, Chen M, Hao Y (2012) High efficient removal of Pb(II) by amino-functionalized Fe_3O_4 magnetic nano-particles. Chem Eng J 191: 104–111

Taty-Costodes VC, Fauduet H, Porte C, Delacroix A (2003) Removal of Cd(II) and Pb(II) ions, from aqueous solutions, by adsorption onto sawdust of *Pinus sylvestris*. J Hazard Mater 105:121–142

Wang Y, Chen H, Xu Y, Sun J, Bai L, Qu R, Wang D, Yu L (2015) Synthesis of polyvinyltetrazole resin by combination of RAFT polymerization and click chemistry for adsorption of Hg(II). J Macromol Sci A 52:707–712

Weber WJ, Morris JCJC (1963) Kinetics of adsorption on carbon from solution. J Sanit Eng Div ASCE 89:31–60

White BR, Stackhouse BT, Holcombe JA (2009) Magnetic γ-Fe_2O_3 nanoparticles coated with poly-L-cysteine for chelation of As(III), Cu(II), Cd(II), Ni(II), Pb(II) and Zn(II). J Hazard Mater 161:848–853

Xia T, Guan Y, Yang M, Xiong W, Wang N, Zhao S, Guo C (2014) Synthesis of polyethylenimine modified Fe_3O_4 nanoparticles with immobilized Cu^{2+} for highly efficient proteins adsorption. Colloid Surf A 443:552–559

Yılmaz Ş, Şahan T, Karabakan A (2017) Response surface approach for optimization of Hg(II) adsorption by 3-mercaptopropyl trimethoxysilane-modified kaolin minerals from aqueous solution. Korean J Chem Eng 34:2225–2235